Boundary-Layer Meteorology (2005) 115: 105–130

UTILITY OF ASSIMILATING SURFACE RADIOMETRIC TEMPERATURE OBSERVATIONS FOR EVAPORATIVE FRACTION AND HEAT TRANSFER COEFFICIENT RETRIEVAL

WADE T. CROW* and WILLIAM P. KUSTAS
USDA ARS, Hydrology and Remote Sensing Laboratory, Room 104, Building 007, BARC-W, Beltsville, MD 20705, U.S.A.

(Received in final form 9 July 2004)

Abstract. Recent advances in land data assimilation have yielded variational smoother techniques designed to solve the surface energy balance based on remote observations of surface radiometric temperature. These approaches have a number of potential advantages over existing diagnostic models, including the ability to make energy flux predictions between observation times and reduced requirements for ancillary parameter estimation. Here, the performance of a recently developed variational smoother approach is examined in detail over a range of vegetative and hydrological conditions in the southern U.S.A. during the middle part of the growing season. Smoother results are compared with flux tower observations and energy balance predictions obtained from the two-source energy balance model (TSM). The variational approach demonstrates promise for flux retrievals at dry and lightly vegetated sites. However, results suggest that the simultaneous retrieval of both evaporative fraction and turbulent transfer coefficients by the variational approach will be difficult for wet and/or heavily vegetated land surfaces. Additional land surface information (e.g. leaf area index (L_{AI}) or the rough specification of evaporative fraction bounds) will be required to ensure robust predictions under such conditions. The single-source nature of the variational approach also hampers the physical interpretation of turbulent transfer coefficient retrievals. Intercomparisons between energy flux predictions from the variational approach and the purely diagnostic TSM demonstrate that the relative accuracy of each approach is contingent on surface conditions and the accuracy with which L_{AI} values required by the TSM can be estimated.

Keywords: Data assimilation, Surface energy fluxes, Surface radiometric temperature, Turbulent transfer coefficients.

1. Introduction

Accurate estimates of energy and momentum fluxes between the surface of the earth and the atmospheric boundary layer are of critical importance for a wide range of agricultural, hydrological, and meteorological applications. Efforts to estimate the magnitude of surface fluxes are frequently frustrated by large amounts of land surface heterogeneity and the need to obtain model inputs at high spatial resolutions. These needs can likely be met only with remote sensing. Consequently, a number of models have been developed to estimate surface energy fluxes based on remote observations of the land surface (see e.g., Norman et al., 1995; Bastiaansen et al., 1998; Jiang and

* E-mail: wcrow@hydrolab.arsusda.gov

Islam, 2001; Su, 2002). These approaches generally utilize surface radiometric temperature (T_s) observations to solve the surface energy balance and partition incoming radiation into various flux components. They are typically diagnostic in nature and therefore make flux predictions only for instances in which T_s observations are available. Obtaining reliable surface energy flux predictions also requires knowledge of ancillary land surface parameters such as the leaf area index (L_{AI}), surface roughness, and the fractional coverage of vegetation (f_v) to accurately estimate near-surface resistance to the transfer of momentum, energy, and water. These parameters are often estimated using remotely observed visible and infrared spectral indices in order to minimize the amount of *in situ* observations required by the energy balance algorithm.

In contrast to diagnostic approaches where surface radiometric temperature is treated as a forcing variable, a number of recent approaches have instead focused on the variational assimilation of T_s into a force-restore equation for surface temperature (Castelli et al., 1999; Boni et al., 2000). These approaches have a number of advantages over purely diagnostic approaches. Most importantly, they provide flux estimates that are continuous in time and can temporally interpolate, using a physically realistic force-restore prognostic equation, between sparse T_s observations (Boni et al., 2001). In addition, estimates of ground heat flux can be obtained using a physically based approach instead of relying on empirical formations that estimate ground heat flux as a fixed fraction of net radiation. A third advantage for variational assimilation-based techniques has recently been described by Caparrini et al. (2003, 2004) who attempt to simultaneously retrieve both turbulent transfer coefficients and daily-averaged evaporative fraction (E_F) magnitudes from T_s observations. A simultaneous retrieval of both variables eliminates the need for the *a priori* specification of surface roughness lengths to obtain transfer coefficient estimates. To date, retrievability concerns have limited the approach to a single-source geometry for surface radiative emission. In contrast, the disaggregation of surface emission into soil and vegetation components is often viewed as a critical component of other models. Diagnostic approaches such as the two-source energy balance model (TSM) (Norman et al., 1995) are based on the disaggregation of T_s observations into soil and vegetative contributions and the separate calculation of soil and canopy energy fluxes. This separation eliminates the need to obtain bulk surface transfer coefficients that attempt to aggregate across soil and vegetation surface components.

Currently, the most advanced operational approaches for regional-scale energy flux monitoring are based on the application of TSM principles to geostationary satellite T_s observations and the independent estimation of leaf area index and surface roughness length (Diak et al., 2004). Because of its reduced parameter requirements, the variational smoother approach of Caparrini et al. (2003, 2004) offers an attractive alternative but has not been extensively tested over a wide range of land surface conditions. The purpose of this study is to evaluate the approach of Caparrini et al. (2003, 2004) during the growing season over a range of different land cover types within the south-central and south-western U.S.A. Three aspects of the approach will be examined: its ability to uniquely and unambiguously retrieve both surface energy fluxes and turbulent transfer coefficients in a simultaneous manner from a time series of T_s observations; the degree to which transfer coefficients derived by the model can be physically interpreted; and the accuracy of its energy flux predictions. The examination of model accuracy and interpretability will be aided by comparison with flux tower observations and TSM predictions at the same series of sites.

2. Energy Balance Models

Analysis is based on the variational smoother approach of Caparrini et al. (2003, 2004) utilizing the force-restore equation for surface temperature (VAR-FR) and the diagnostic TSM of Norman et al. (1995). Both models are based on the remote observation of T_s and the surface energy balance equation that describes the partitioning of incoming net radiation (R_n) into latent energy (LE, L being the latent heat of vaporization and E the evaporation), sensible heating (H), and ground heat flux (G) components:

$$R_n = LE + H + G. \tag{1}$$

Details underlying both approaches are described below.

2.1. Variational data assimilation approach

As noted above, the VAR-FR approach is based on the use of a force-restore equation to model the evolution of surface soil temperature (T_s) in response to variations in radiative forcing ($R_n - H - LE$) occurring at a diurnal frequency (ω):

$$\frac{dT_s}{dt} = \frac{2\sqrt{\pi\omega}}{P}[R_n - H - LE] - 2\pi\omega(T_s - T_d), \tag{2}$$

where P is the thermal inertia of the land surface and T_d the deep soil temperature. The approach of Caparrini et al. (2003, 2004) rewrites (2) by defining the evaporative fraction (E_F) to be:

$$E_F = \frac{LE}{LE + H}, \tag{3}$$

and utilizing a bulk transfer formulation for H where:

$$H = \rho c_p C_H U(T_s - T_a) \tag{4}$$

and T_a is the air temperature, U the wind speed, c_p is the specific heat of air, ρ the density of air, and C_H the bulk transfer coefficient for heat. Stability impacts on C_H can then be described as a function of the bulk Richardson number, Ri_B:

$$\frac{C_H}{(C_H)_N} = 1 + e^{\Psi}(1 - e^{10Ri_B}), \tag{5}$$

where Ψ is the static stability correction parameter and the neutral transfer coefficient $(C_H)_N$ is typically represented as:

$$(C_H)_N = \frac{k^2}{\ln(z_{ref}/z_{0m})\ \ln\ (z_{ref}/z_{0h})} \tag{6}$$

with k representing Van Karman's constant, z_{ref} the measurement height for wind, and z_{0m} and z_{0h} roughness lengths for momentum and heat transfer, respectively.

Substracting one from both sides of (3) and solving for $H + LE$ leads to $H + LE = H/(1 - E_F)$. Inserting this expression into (2) and expanding H via (4) and (5) yields:

$$\frac{dT_s}{dt} = \frac{2\sqrt{\pi\omega}}{P}\left(R_n - \frac{(C_H)_N}{1 - E_F}[T_s - T_a]\rho c_p U[1 + e^{\Psi}(1 - e^{10Ri_B})]\right) - 2\pi\omega(T_s - T_d). \tag{7}$$

Variables P and Ψ are considered to be non-time varying and set equal to 750 J m^{-2} K^{-1} $s^{-1/2}$ and ln (2) respectively for all sites. While these values are somewhat uncertain, off-line sensitivity results demonstrate the limited sensitivity of E_F results to variations in either parameter. The restoring temperature T_d is calculated by applying a semi-diurnal (12-h) filter to T_s observations using a phase lag of 2 h. Values for R_n, U, Ri_B, and T_a are taken from micrometeorological observations and the definition of the bulk Richardson number:

$$Ri_B = \frac{g}{\theta}\frac{\Delta\theta z_{ref}}{U^2}, \tag{8}$$

where g is the gravitational constant, θ the potential temperature of the air, and $\Delta\theta$ the air/surface potential temperature difference. In this study T_s observations are derived from a ground-based infrared radiative thermometer. However, the expectation is that satellite measurements will eventually be utilized. The VAR-FR model is a single-source model in the sense that contributions from soil background to T_s observations are neglected and observations of T_s are directly inserted into (4).

Given a times series of daytime T_s observations, Caparrini et al. (2003, 2004) describe a variational data assimilation system (VAR-FR) capable of simultaneously retrieving estimates of both $(C_H)_N$ and E_F. The variational problem is solved by obtaining an adjoint state model for (7) and utilizing the model to efficiently search for values of $(C_H)_N$ and E_F that minimize the root-mean-squared difference between predictions of T_s obtained via (7) and T_s observations (Castelli et al., 1999). The approach is applied over discrete (multi-day) time periods within which E_F is allowed to vary daily and $(C_H)_N$ is held constant. Due to the self-preservation properties of E_F (Crago and Brutsaert, 1996), diurnal variation in E_F is assumed small and neglected. In order to eliminate the possibility of negative $(C_H)_N$ retrievals, Caparrini et al. (2003, 2004) solve for the transformed parameter R defined to be:

$$(C_H)_N = e^R. \tag{9}$$

The VAR-FR also requires an *a priori* specification of physically realistic limits for E_F. Also otherwise noted, a range of between 0.1 and 0.9 is used.

2.2. The two-source model

A detailed description of the original TSM can be found in Norman et al. (1995). The modelling approach evaluates the temperature contribution of the vegetated canopy layer and soil/substrate to the radiometric surface temperature observation, and the resulting turbulent heat flux contributions driven by surface–air temperature differences with aerodynamic resistance parameterizations for the vegetation and soil components. This modelling strategy follows the conceptual two-source framework proposed by Shuttleworth and Wallace (1985) for partially vegetated surfaces (see also Shuttleworth and Gurney, 1990).

There have been several modifications to the original TSM formulation that can significantly influence flux predictions for partial canopy covered surfaces. These include estimating the divergence of net radiation through the canopy layer with a more physically based algorithm, adding a simple method to address the effects of clumped vegetation on radiation divergence and wind speed inside the canopy layer, adjusting the magnitude of the Priestley–Taylor (Priestley and Taylor, 1972) coefficient used in estimating canopy transpiration, and formulating a new estimation for soil resistance to sensible heat-flux transfer (Kustas and Norman, 1999a, b; 2000a, b).

The TSM and VAR-FR approaches present a number of key differences. The TSM approach uses T_s as a forcing variable to solve a diagnostic set of equations that considers the impact of thermal emission from both the canopy and soil. For the 4-h period on either side of solar noon, the TSM model assumes ground heat-flux fraction (G_F) to be a function of L_{AI}, R_n, and solar zenith angle θ_s (Norman et al., 1995; Anderson et al., 1997):

$$G_F = G/R_n = c_g \exp\left(-\kappa L_{AI}/\sqrt{2\cos\theta_s}\right). \tag{10}$$

Following Kustas et al. (1998), c_g is typically assumed to be 0.35 and the extinction coefficient κ set to 0.6. Since G_F is modelled as a simple function of L_{AI} and canopy heat storages are neglected, the TSM does not require the forward temporal integration of any thermal state. Flux calculations are made based solely on instantaneous micrometeorological observations, plus vegetation structure and T_s. The roughness length for momentum is taken to be one-eighth of plant canopy height. Accurate L_{AI} estimates for the vegetation canopy must be independently obtained in order to calculate the relative contribution of vegetative and soil sources to T_s observations, the net radiation partitioning between the vegetation canopy and soil, and the aerodynamic resistance to momentum transfer within the canopy.

In contrast, the VAR-FR attempts to solve for the heat transfer coefficient and surface energy fluxes (including G) by assimilating T_s observations into a prognostic force-restore equation for canopy temperature (7). Unlike the TSM, memory of past thermal states is retained in the deep temperature state T_d. However, as a single-source approach, it neglects the impact of background soil emission on T_s observations.

3. Study Locations and Data

Site locations, surface conditions, and dates are listed in Table I; measurements of surface energy fluxes, micrometeorological quantities, and surface radiometric temperature are available at all sites. Data at the MONSOON1 and MONSOON5 sites were collected as part of the MONSOON'90 field experiment (Kustas and Goodrich, 1994) in the U.S. Department of Agriculture Agricultural Research Service's Walnut Gulch experimental watershed near Tombstone, Arizona. The LW site was maintained as a long-term

TABLE I
Study site characteristics.

Site	Lat/long	Julian days	Year	Land cover	NDVI	$\overline{E_F}$
ELRENO1	35.54/−98.02	175–195	1997	Pasture	0.61	0.83
ELRENO13	35.56/−98.06	171–195	1997	Bare soil	0.00	0.50
MONSOON1	31.74/−110.05	209–222	1990	Sparse shrubs	0.20	0.55
MONSOON5	31.73/−109.94	210–221	1990	Sparse grass	0.35	0.60
FIFE	39.00/−96.50	169–194(wet)	1987	Native prairie	0.70	0.86
		194–219(dry)	1987	Native prairie	0.61	0.65
LW	36.60/−97.48	149–188(wet)	1997	Range	0.30	0.53
		188–228(dry)	1997	Range	0.30	0.43

energy flux study site between 1996 and 1998 by the National Oceanic and Atmospheric Administration/Atmospheric Turbulence and Diffusion Division within the Little Washita (LW) river basin in south-central Oklahoma. The ELRENO1 and ELRENO13 sites in the vicinity of El Reno, Oklahoma were instrumented as part of the 1997 Southern Great Plains Hydrology Experiment. Site details can be found in Hollinger and Daughtry (1999) and in SGP'97 documentation accessible online at http://hydrolab.arsusda.gov/sgp97/documents.html

Data collected at the MONSOON, LW, and ELRENO sites are based on observations made on single flux towers. In contrast, data for the First International Satellite Land Surface Climatology Project (ISLCP) Field Experiment (FIFE) site are based on the areal average of several flux towers within the 15^2-km^2 FIFE study site (Sellers et al., 1992) in eastern Kansas. Acquisition, processing, and spatial averaging of the FIFE dataset is detailed in Betts and Ball (1998). Flux observations at the MONSOON sites had previously been modified to ensure energy balance by solving for LE as a residual (Kustas et al., 1994). At the ELRENO and LW sites, raw flux observations were considered only from days exhibiting a daytime closure ratio, $(LE + H)/(R_n - G)$, greater than 0.75.

Within the south-central and south-western U.S.A., middle to late parts of the growing season (June to August) typically exhibit the most complex temporal interaction between periods of energy- and water-controlled evapotranspiration, the most profound impact of water stress on vegetation health and productivity, and the strongest contrasts between soil and vegetation temperatures. As a consequence, prediction of surface energy fluxes based on T_s observations during this period is both difficult and highly relevant for agricultural and land management applications. In our analysis, site locations and times were selected to capture the full range of growing season hydrologic and vegetation conditions typically encountered in the region. Normalized difference vegetation index (NDVI) values at the sites range from essentially zero at the bare soil ELRENO13 site to 0.70 at the FIFE site. Average daytime E_F observations range between 0.43 for arid conditions encountered at the rangeland LW site to 0.86 for observations collected during a wet period at the native prairie FIFE site. Measurements of daytime-averaged (1000–1600 CST) turbulent energy fluxes range between 100 and 400 W m^{-2} for H and 100 and 500 W m^{-2} for LE.

4. Results

A fundamental concern about application of variational techniques to any geophysical problem is whether the approach is capable of making unambiguous and physically interpretable predictions of variables. If so, then a secondary question arises as to how accurate these retrievals are relative to independent measurements and competing approaches. To this end, the approach of Caparrini et al. (2003, 2004) was evaluated at sites listed in Table I based on its ability to simultaneously retrieve both E_F and $(C_H)_N$ (Section 4.1), the physical interpretability of its $(C_H)_N$ predictions (Section 4.2), and its ability to accurately estimate E_F (Section 4.3). Accuracy comparisons for E_F retrievals were made relative to both independent flux tower observations as well as comparable TSM predictions obtained at the same series of sites. All comparisons to measurements were made based on daytime-averaged (1000–1600 local time) energy flux values.

4.1. Simultaneous retrieval of E_F and $(C_H)_N$

Using the adjoint-based variational data assimilation strategy of Caparrini et al. (2003, 2004) (VAR-FR), E_F and R predictions were calculated at each of sites listed in Table I. Based on optimization against a time series of T_s observations, the VAR-FR algorithm provides output for a separate E_F value for each day in the assimilation period and a single R prediction that defines the heat transfer coefficient for the entire period. Averaging daily E_F predictions within a given assimilation yields the period averaged evaporative fraction ($\overline{E_F}$). Figure 1 plots iterative ($\overline{E_F}$) and R values obtained as the adjoint-based variational approach searches for a minimum at the MONSOON1 site, and Figure 2 shows the minimization of T_s root-mean-square-error (RMSE) as a function of iteration number for the four initial conditions shown in Figure 1a. Initial conditions were arbitrarily selected to span a range of possible land surface conditions. The VAR-FR system converges to a relatively flat valley after 1000 iterations (Figures 2c and 3), which expresses a trade-off between cooling of the surface via turbulent transfer and evapotranspiration. Highly negative R values imply smooth surfaces and vigorous evapotranspiration. Larger (less negative) R values imply rougher surfaces with increased reliance on turbulent heat transfer for cooling. Convergence beyond iteration number 1000 (approximately) is extremely slow (Figure 1d) and associated with essentially negligible variations in T_s RMSE (Figure 2). Each of the four convergence pathways in Figure 2 is likely to satisfy any reasonable convergence criterion before iteration number 2500. Nevertheless, large differences in R and $\overline{E_F}$ retrievals persist between pathways beyond 5000 iterations (Figure 1d). This suggests that optimized R and $\overline{E_F}$ values will vary as a function of initial conditions (Figure 1a) unless extremely strict convergence criterion is utilized.

In order to overcome convergence problems associated with the simultaneous optimization of both R and E_F, the approach of Caparrini et al. (2003, 2004) was modified so that E_F values were separately optimized for a range of

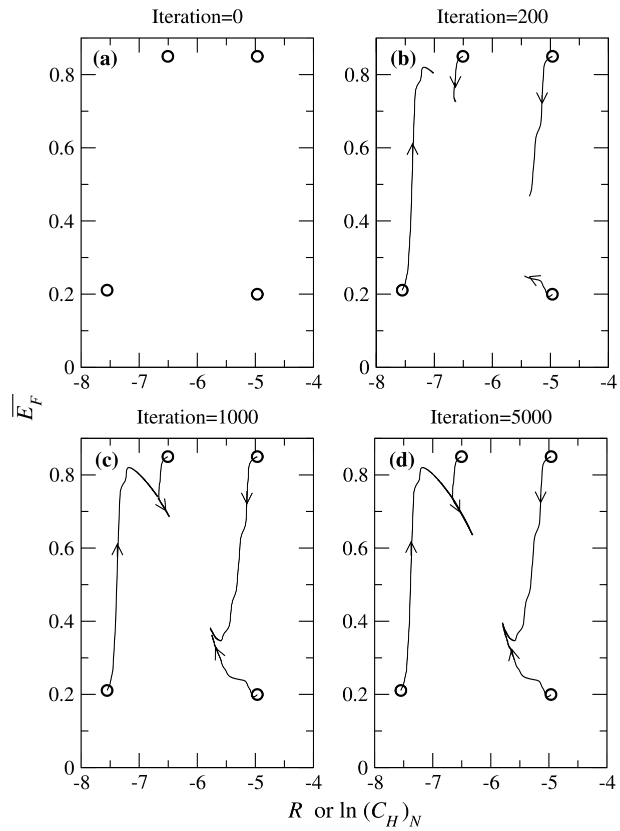

Figure 1. Iterative evolution R and $\overline{E}_F$ retrivals by the VAR-FR approach at the MONSOON1 site. Initial conditions for the iterative solver are indicated with open circles.

fixed R values. Optimization yields a time series of E_F predictions associated with the best fit to observed T_s values for a fixed value of R. In this case, convergence was good after 100 iterations of the algorithm. Figure 3a plots the temporal average of E_F values ($\overline{E_F}$) required to minimize the model T_s error over a range of R values at four sites listed in Table I: ELRENO13, LW(dry), MONSOON1, and FIFE(wet). Figure 3b shows T_s RMSE differences between observed and modelled T_s for the same range of R. The simultaneous retrieval of both E_F and R requires the presence of well-defined minima in T_s RMSE to allow for the unambiguous specification of R values. However, observed T_s minima at the LW(dry) and FIFE(wet) sites are shallow with respect to variations in R (Figure 3b) and lend uncertainty to optimized R values. This ambiguity can have major impacts on the subsequent accuracy of E_F predictions (Figure 3c). For instance, during the LW(dry) period, R values between -6.25 and -5.25 produce essentially the same fit to T_s observations yet lead to E_F RMSE that vary between 0.1 and

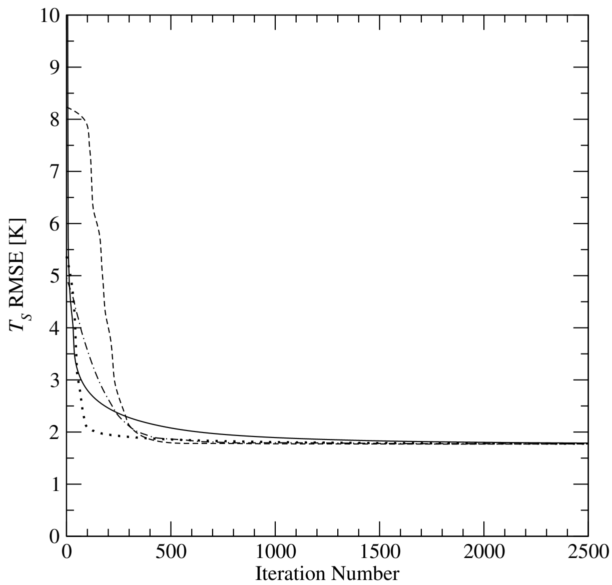

Figure 2. Decrease in T_s RMSE as a function of VAR-FR iteration number for the four initial conditions shown in Figure 1.

0.3. At the FIFE(wet) site, very good fits to both T_s and E_F observations are associated with an R value near -4.5. However, larger (less negative) values of R produce essentially identical fits to T_s observations and are associated with a poorer E_F accuracy. At both sites, T_s observations do not unambiguously identify R values associated with accurate E_F predictions. This lack of identifiability is the ultimate source of convergence problems encountered when R and E_F are simultaneously optimized (Figures 1 and 2).

Some amount of additional land surface information appears necessary to unambiguously retrieve both E_F and R at these sites. This information need not be detailed to offer substantial improvement. For instance, following Garratt and Hicks (1973) and assuming $\ln(z_{0m}/z_{0h}) \approx 2$ in (6), a z_{0m} value of 0.5 m corresponds to an R value of -4.2 at the native prairie FIFE site. Such a roughness length is significantly larger than the 0.01–0.03 m range estimated from micrometeorological observations at the same site (Verma et al., 1992) and can be rejected as physically unrealistic given even cursory knowledge of FIFE land cover conditions. Nevertheless, limiting R retrievals to $R > -4.2$ substantially improves VAR-FR E_F predictions at the site (E_F RMSE of 0.10 versus 0.30).

4.1.1. *Role of E_F Variability*

Figure 4 examines this retrievability issue in detail at the MONSOON1 site. The force-restore equation for surface temperature, (7), predicts that, for

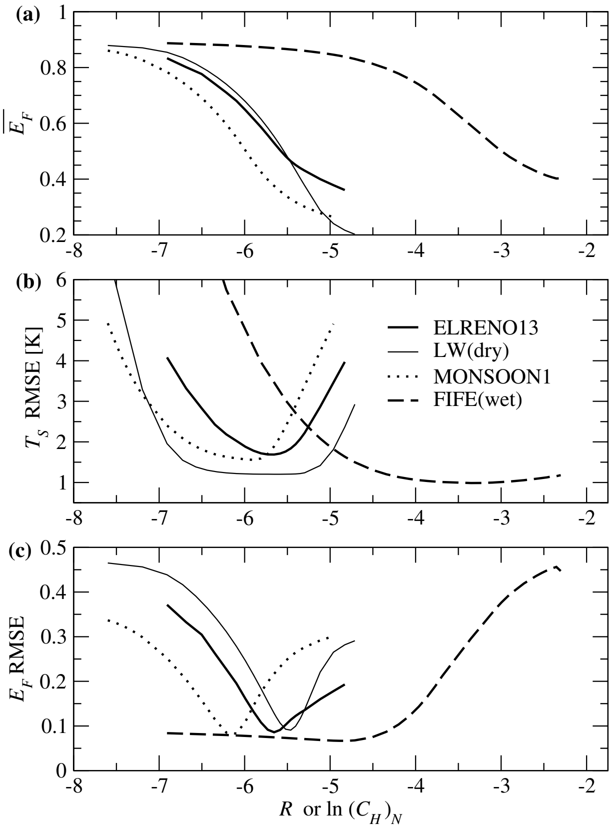

Figure 3. Values of (a) $\overline{E}_F$, (b) T_s RMSE, and (c) E_F RMSE associated with the best fit to T_s observations found by the VAR-FR algorithm for a range of pre-specified values of R.

similar meteorological and R_n conditions, changes in $(C_H)_N$ and E_F will produce identical T_s temporal variations provided the ratio $(C_H)_N/(1 - E_F)$ is conserved. As a consequence, an optimal value of this ratio can be maintained for any pre-specified value of $(C_H)_N$ via the appropriate adjustment of E_F. Figure 4a plots the average of $(C_H)_N/(1 - E_F)$ within the assimilation period, $(C_H)_N/(1 - \overline{E_F})$, for a range of pre-specified R values. In the vicinity of the observed T_s RMSE minimum (see Figure 4b), the VAR-FR algorithm compensates for changes in $(C_H)_N$ by adjusting E_F (Figure 4c) and maintaining nearly optimal $(C_H)_N/(1 - \overline{E_F})$ levels. Values of $(C_H)_N/(1 - \overline{E_F})$ deviate significantly from optimal levels only when E_F values required for optimal fitting to T_s observations fall outside the pre-specified E_F bounds. In this case, the data assimilation system is forced to truncate E_F retrievals and is prevented from obtaining an optimal fit to T_s observations (Figure 4b). If E_F values are prevented from becoming optimally large (small), model T_s predictions become too high (low) and $(C_H)_N$ values can be rejected based on

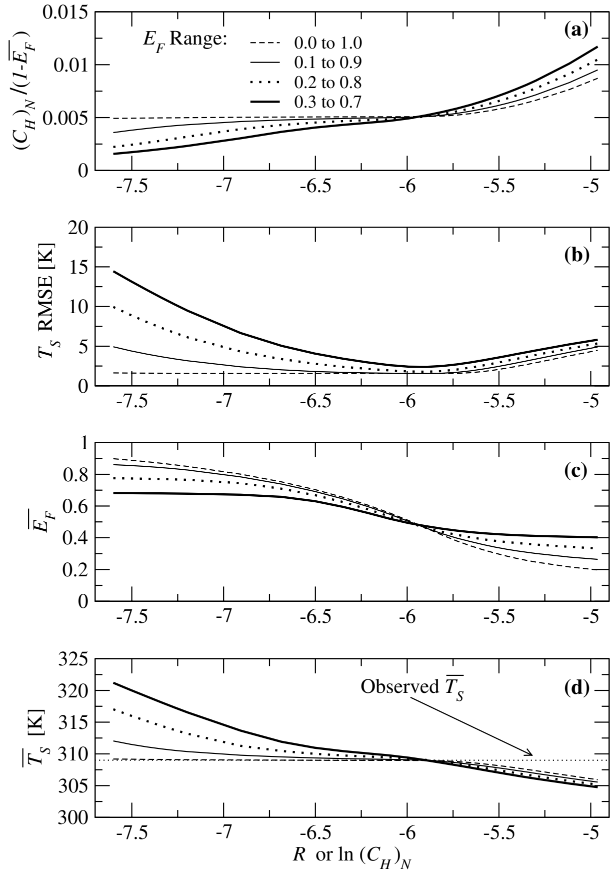

Figure 4. For the MONSOON1 site, values of (a) $(C_H)_N/(1-\overline{E}_F)$, (b) T_s RMSE, (c) $\overline{E}_F$ and (d) $\overline{T}_s$ associated with the best fit to T_s observations found by the VAR-FR algorithm for a range of pre-specified values for R and different E_F retrieval bounds.

their inability to match T_s observations (Figure 4d). The larger the range of E_F deemed acceptable, however, the more latitude the variational approach has to adjust E_F with impunity and the shallower the T_s RMSE minimum. Consequently, the simultaneous retrieval of $(C_H)_N$ and E_F is dependent on the *a priori* restriction of E_F to a certain bounded range. These bounds should reflect knowledge of a site's vegetation and climatic characteristics. For instance, dense vegetation at the FIFE site virtually guarantees an E_F value above 0.5. Consequently, restricting the E_F range to between 0.5 and 0.9 (as opposed to between 0.1 and 0.9), substantially improves the retrievability of $(C_H)_N$ at the FIFE(wet) site and reduces E_F RMSE by 50% (0.29 to 0.15). In contrast, restricting E_F predictions to a lower range, say between 0.3 and 0.7, is inconsistent with the site's vegetation and climatic characteristics and does not lower the E_F RMSE (0.30 versus 0.29).

Since $\overline{E_F}$ is simply an averaged value obtained within the entire assimilation period, deviations from the optimal $(C_H)_N/(1-\overline{E_F})$ level occur before temporally averaged $\overline{E_F}$ values approach these limits (Figure 4d). Extreme E_F conditions within the assimilation period encroach upon feasible E_F bounds and provide instances in which good T_s fits cannot be accommodated for certain values of $(C_H)_N$ without resorting to physically unrealistic E_F values. The presence of variability within the assimilation period, and/or more tightly bounded ranges for realistic E_F values, enhances retrievability by presenting cases where extreme values of E_F are required to match T_s observations. If these values fall outside of the physically realistic bounds for E_F, specific values of $(C_H)_N$ can be labeled as non-optimal. Retrievability can also be enhanced by employing longer assimilation windows that encompasses greater E_F variability within the assimilation period.

4.1.2. *Role of Land Surface Conditions*

Figure 5 plots values for $(C_H)_N/(1-\overline{E_F})$ that lead to T_s RMSE minima at each site; results for all eight sites are plotted in order of decreasing NDVI values for Table I. Large variations are observed between sites. The magnitude of this ratio, along with P, determines the vigour of diurnal variations in T_s due to the periodic radiative forcing of the land surface. High (low) $(C_H)_N/(1-\overline{E_F})$ fractions are typical of wet and highly vegetated (dry and sparsely vegetated) sites where diurnal T_s dynamics are (pronounced) damped. Setting an optimal value of this fraction equal to some constant K, solving for $\overline{E_F}$, and taking the derivative of $\overline{E_F}$ with respect to $(C_H)_N$ yields:

$$\frac{d\overline{E_F}}{d(C_H)_N} = -K^{-1}. \tag{11}$$

A highly negative $dE_F/d(C_H)_N$ (i.e. a small optimal $(C_H)_N/(1-\overline{E_F})$ value) dictates that large variations in $(C_H)_N$ will require analogously large adjustments in $\overline{E_F}$ to minimize T_s RMSE. Consequently, a large variation in $(C_H)_N$ cannot be accommodated without exceeding pre-set E_F bounds. This inflexibility enhances the retrievability of $(C_H)_N$. This is typically the case with dry and sparsely vegetated sites given in Table I and Figure 5 that exhibit low $(C_H)_N/(1-\overline{E_F})$ and, by (11), highly negative $dE_F/d(C_H)_N$. Note the poor retrievability in Figure 3 for the heavily vegetated FIFE site during a wet period relative to the lightly vegetated and drier ELRENO13 and MONSOON1 sites.

4.1.3. *Diagnostics for Retrievability*

Results in Sections 4.1.1 and 4.1.2 suggest the potential of two simple diagnostics to evaluate the potential of the Caparrini et al. (2003, 2004) approach at a given site. The averaged magnitude of $T_s - T_a$ provides a

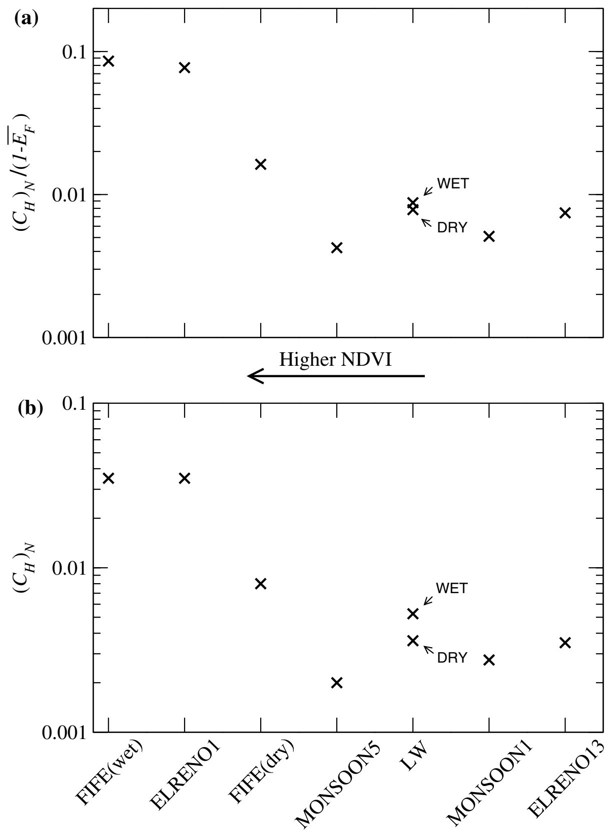

Figure 5. (a) $(C_H)_N/(1-\overline{E}_F)$ and (b) $(C_H)_N$ values associated with the best fit to T_s observations for all sites listed in Table 1.

measure of land surface cooling efficiency and the magnitude of $(C_H)_N/(1-\overline{E_F})$ values required to match T_s observations. Smaller optimal values of $(C_H)_N/(1-\overline{E_F})$ dictate more highly negative $dE_F/d(C_H)_N$ values and less pronounced T_s minima. Likewise, since $(C_H)_N$ is constant within assimilation periods, variations in $T_s - T_a$ manifest themselves as day-to-day variability in E_F. Larger variability in E_F, in turn, reduces the range of $(C_H)_N$ values that yields E_F predictions within physically realistic ranges. For Figure 6, the sharpness of the T_s minimum at all eight sites listed in Table I was defined as the absolute range of $(C_H)_N$ values whose T_s RMSE is within 0.2 K of the global T_s RMSE minimum. Each site is ranked according to this sharpness measure. The size of the circles in Figure 6 reflects this ranking, with larger circles assigned to sites with well-defined T_s RMSE minimum. Circles are positioned in the plot according to mean daytime $T_s - T_a$ and the magnitude of day-to-day variations in daytime-averaged $T\text{s} - T_a$. There exists a tendency for sites with higher mean $T_s - T_a$ and greater $T\text{s} - T_a$ variability to

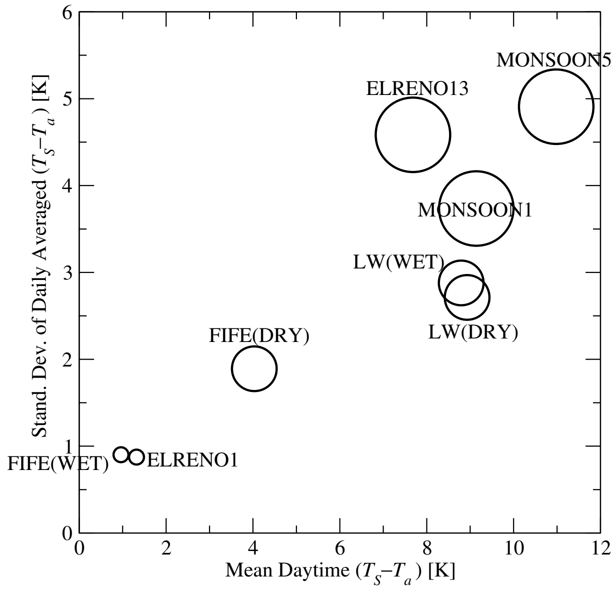

Figure 6. Relationship between retrievability of $(C_{\mathrm{H}})_{\mathrm{N}}$ and the mean and standard deviation of daytime-averaged $T_{\mathrm{s}} - T_{\mathrm{a}}$ differences. Circle size is determined by ranking sites according to the range of $(C_{\mathrm{H}})_{\mathrm{N}}$ found within 0.2 K of the T_{s} RMSE minimum. Larger circles have smaller $(C_{\mathrm{H}})_{\mathrm{N}}$ ranges and the best retrievability.

enjoy sharper T_{s} RMSE minima and improved prospects for the simultaneous retrieval of both $(C_{\mathrm{H}})_{\mathrm{N}}$ and E_{F}. Since T_{s} and T_{a} observations represent the key drivers for VAR-FR model predictions, these two diagnostics (the mean and standard deviation of $T_{\mathrm{s}} - T_{\mathrm{a}}$) appear to drive site-to-site variations in the retrievability of $(C_{\mathrm{H}})_{\mathrm{N}}$.

4.2. Physical interpretability of $(C_{\mathrm{H}})_{\mathrm{N}}$ retrievals

A well-known drawback for one-source energy balance approaches is the non-equivalence of the aerodynamic and radiative temperatures, the latter being strongly influenced by the areal fraction of bare soil viewed by the radiometer (Kustas et al., 2004). Direct measurement of both soil (T_{soil}) and vegetation (T_{veg}) surface radiometric temperatures at the MONSOON1 and MONSOON5 sites provides an opportunity to study partial vegetation impacts on VAR-FR $(C_{\mathrm{H}})_{\mathrm{N}}$ retrievals. Viewing of the surface at different 'look' angles leads to variations in the fraction of observed thermal emission originating from the canopy (f_v) and variations in the relative weighting of soil and vegetation sources underlying remote T_{s} observations. Assuming equal emissivities for vegetation and soil, the radiometric temperature T_s can be related to T_{soil}, T_{veg}, and f_v via the following approximate relationship:

$$T_s \approx [f_s T_{veg}^4 + (1 - f_s) T_{soil}^4]^{0.25}, \tag{12}$$

where f_v varies as a function of both observation 'look' angle and L_{AI}. Using (12), a series of T_s time series were constructed from T_{soil} and T_{veg} measurements assuming various values of f_v. Figure 7 describes the impact of variations in f_v, due ostensibly to changes in view 'look' angle, on VAR-FR E_F and $(C_H)_N$ retrievals at the MONSOON1 site. Viewing partially vegetated surfaces from increasingly high zenith angles (i.e. increasingly further from nadir) leads to increased weighting of vegetation thermal emission and a reduction in the near-surface $T_s - T_a$ value driving turbulent energy fluxes. This cooling increases the magnitude of $(C_H)_N/(1 - E_F)$ required to match T_s observations. Due to temporal E_F variability at the MONSOON1 site that spans the range of physically realistic E_F values, increases in $(C_H)_N/(1 - E_F)$ are most easily accomplished by

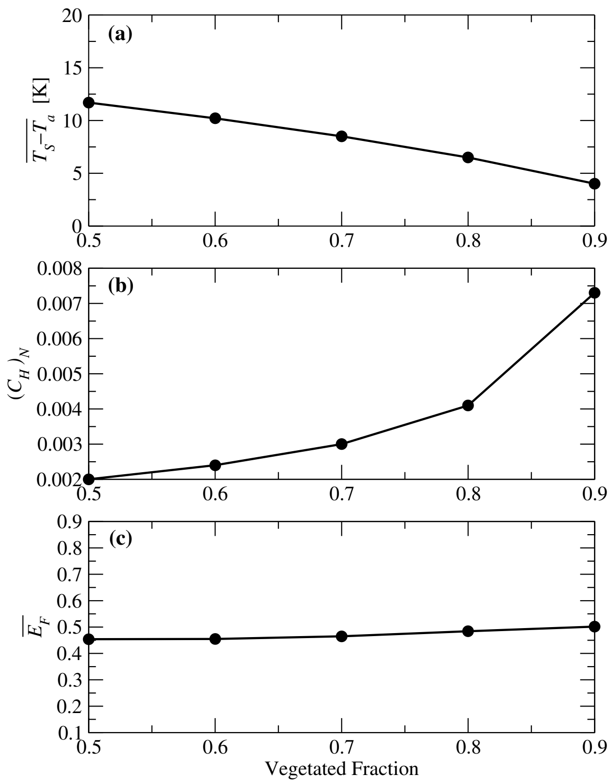

Figure 7. (a) Average $T_s - T_a$ difference, (b) retrieved $(C_H)_N$, and (c) retrieved $\overline{E}_F$ values at the MONSOON1 site for a range of vegetation fractions.

raising $(C_H)_N$ values. These changes are at odds with the formal definition of $(C_H)_N$ in (6) and suggest that values of $(C_H)_N$ retrieved by the one-source VAR-FR approach actually constitute effective transfer parameters, which reflect, in part, viewing geometry and the impact of background soil temperature. In contrast, variations in f_v have relatively little impact on E_F retrievals.

The impact of bare soil emission on $(C_H)_N$ retrievals over partially vegetated canopies is also evident in Figure 5b. Note that lower $(C_H)_N$ (i.e. smoother aerodynamic conditions) are required to match T_s observations for the shrub and grassland MONSOON sites versus the bare soil ELRENO13 site. This runs counter to expectations concerning the aerodynamic roughness at both sites, and most likely reflects the need for anomalously low $(C_H)_N$ values to blunt the impact of very high background soil temperatures at the MONSOON sites.

Irregardless of the physical interpretation for retrieved $(C_H)_N$ values, the VAR-FR approach will return accurate energy flux values if transfer coefficients match effective values of $(C_H)_N$ that minimize E_F error. Figure 8 demonstrates that, with the exception of a very pronounced low bias at high $(C_H)_N$, fitting to T_s values does a relatively good job at recovering $(C_H)_N$ values that minimize E_F RMSE.

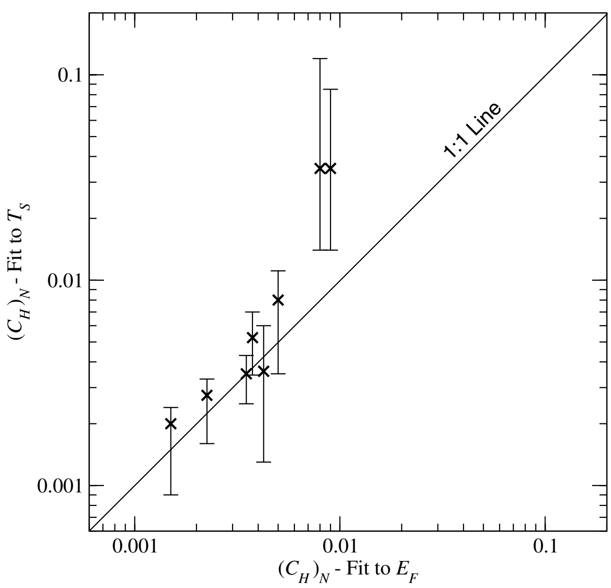

Figure 8. Comparisons between $(C_H)_N$ retrieved by fitting to T_s observations and $(C_H)_N$ values associated with the best E_F predictions. Vertical error bars signify range of $(C_H)_N$ values found within 0.2 K of the T_s RMSE minimum.

4.3. Accuracy of E_F and G_F retrievals

Since R_n values are measured and energy balance assumed, flux results for the VAR-FR approach can be completely described with the normalized fractions E_F, defined in (3), and G_F, defined in (10). Figures 9 and 10 show daytime averaged E_F and G_F predictions made by the VAR-FR method for each study period/site listed in Table I. Dotted lines reflect the spread in E_F and G_F results introduced by considering all R values within 0.2 K of the minimum T_s RMSE, and open circles are flux tower observations. Uncertainty associated with poorly defined T_s minima introduces a significant level of uncertainty into the evaluation of VAR-FR E_F predictions. For instance, VAR-FR results for LW(DRY) demonstrate a good fit to E_F observations

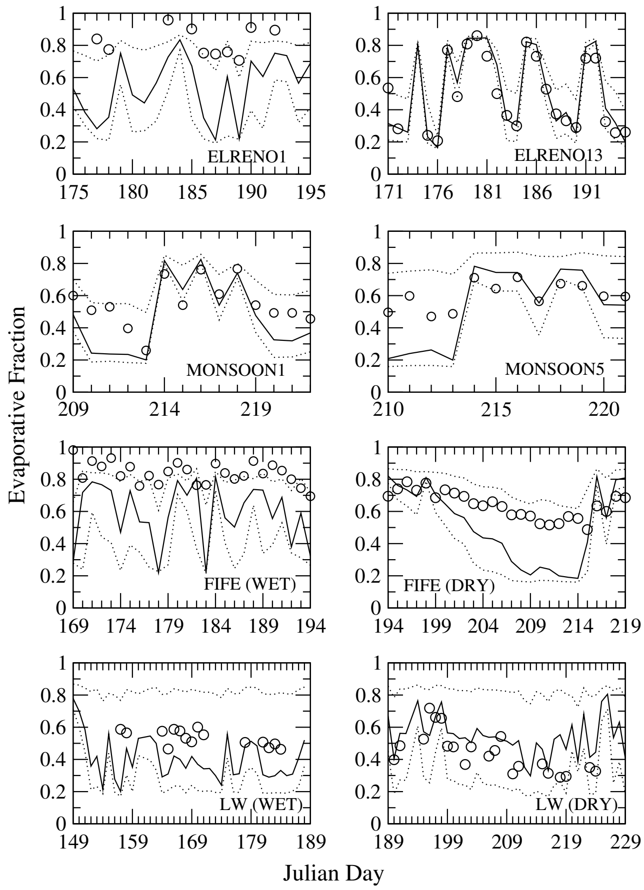

Figure 9. Comparisons between VAR-FR E_F predictions (solid lines) and flux tower observations (open circles). Dotted lines represent the range of E_F predictions associated with T_s RMSE within 0.2 K of the global T_s RMSE minimum.

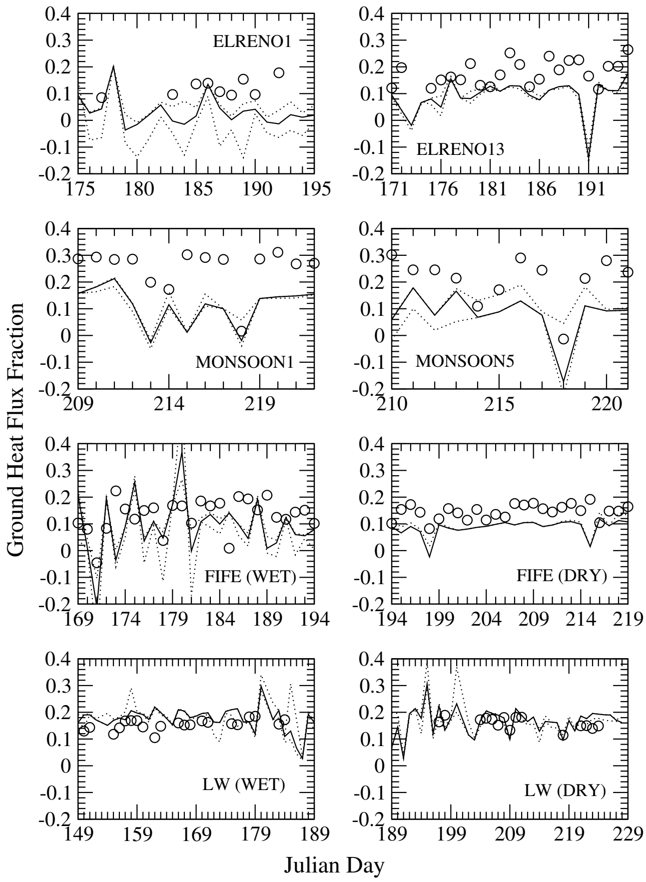

Figure 10. Comparisons between VAR-FR G_F prepdictions (solid lines) and flux tower observations (open circles). Dotted lines represent the range of E_F predictions associated with T_s RMSE within 0.2 K of the global T_s RMSE minimum.

for the $(C_H)_N$ value associated with the best fit to T_s observations (solid line in Figure 9), however essentially identical fits to T_s observations (dotted lines in Figure 9) can produce widely varying, and much worse, E_F predictions. The opposite is true at the FIFE(WET) site where the best fit is associated with low E_F accuracy, but alternative $(C_H)_N$ values, with only a slightly worse fit to T_s, lead to very good E_F retrieval accuracy (see top dotted line in Figure 9 for FIFE(WET)). VAR-FR G_F results are generally more robust to the impact of $(C_H)_N$ uncertainty (note the smaller spread of dotted lines in Figure 10 versus Figure 9) and clearly reveal a low bias when compared to flux tower observations.

Comparison of results in Figures 9 and 10 to competing TSM predictions offers an important perspective on VAR-FR results. Intercomparisons between competing models should reflect underlying differences in model complexity. An attractive characteristic of the VAR-FR model is that it is a parsimonious approach that, in theory, requires little or no ancillary information concerning surface conditions. In contrast, the TSM requires independent estimates of vegetation L_{AI}. These values are often estimated as a function of remote NDVI observations (Choudhury, 1987; Choudhury et al., 1994):

$$L_{AI} = \frac{1}{-\kappa} \ln\left(\frac{\mathrm{NDVI}_{max} - \mathrm{NDVI}}{\mathrm{NDVI}_{max} - \mathrm{NDVI}_{min}}\right), \tag{13}$$

where κ is assumed to be 0.8 and NDVI_{min} (NDVI of bare soil) to be 0.00. NDVI_{max} (NDVI at 100% vegetation cover) values were assumed equal to 0.65 at the LW and ELRENO sites (French et al., 2003), 0.75 at the FIFE site, and 0.60 at the MONSOON sites. The roughness length for momentum transfer was taken to be one-eighth of the observed vegetation height at each site. L_{AI} estimates from (13) were used to calculate G_F at each site via (10) and f_v values used to partition T_s between soil and vegetation sources via (12). Consequently, meaningful comparisons between the TSM and VAR-FR approaches should reflect the ease in which accurate L_{AI} estimates can be obtained from available remote sensing observations. Figures 11 and 12 show E_F and G_F RMSE results for TSM predictions utilizing a range of L_{AI} values. Horizontal lines represent RMSE for comparable VAR-FR retrievals at each site. Dashed vertical lines represent estimates of L_{AI} obtained from satellite-derived NDVI observations listed in Table I and from Equation (13).

Irregardless of the L_{AI} choice, TSM E_F predictions (Figure 11) are superior for wet and heavily vegetated conditions at the ELRENO1 and FIFE(WET) sites. Conversely, VAR-FR E_F predictions are superior for the bare soil ELRENO13 site and dry conditions at the LW site. Using L_{AI} values derived from Table I and from (13) leads to slightly superior TSM results at the MONSOON5, FIFE(DRY), and LW(WET) sites and similar results at the MONSOON1 site. However, large uncertainty associated with VAR-FR E_F predictions (see Figure 9) makes unambiguous E_F intercomparisons impossible. Owing to a reduced uncertainty in VAR-FR results for G_F, intercomparison results for G_F retrievals in Figure 12 can be made with more certainty. Except for the LW site, where optimal L_{AI} values are underestimated by NDVI observations and (13), RMSE G_F results in Figure 12 reveal a tendency for the empirical TSM approach (10) to outperform the VAR-FR model.

Actual turbulent energy fluxes are plotted in Figure 13, where TSM predictions are based on L_{AI} estimates derived from (13). The overestimation of latent heat flux (LE) by the TSM at the ELENO1 site could be exacerbated by energy closure issues, resulting in the underestimation of LE by flux tower observations at the site (Twine et al., 2000). The underestimation of E_F by the

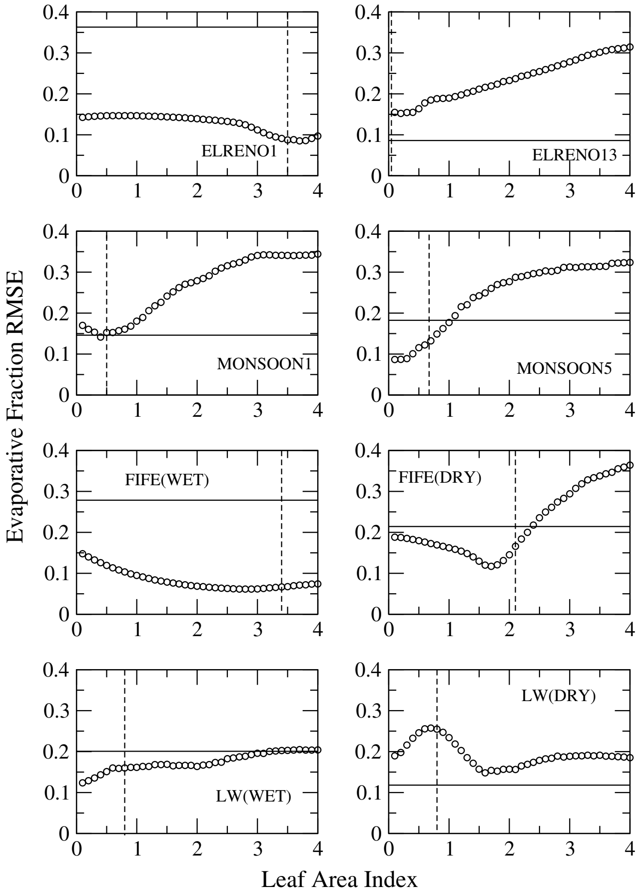

Figure 11. Comparisons between the accuracy of VAR-FR E_F prepdictions (solid horizondal lines) and TSM predictions (open circles) made using a range of L_{AI} values. Dashed vertical lines represent estimates of L_{AI} derived from NDVI values listed in Table 1 and Equation (13).

VAR-FR model at the ELRENO1, LW(WET), and FIFE(WET) sites (see Figure 9) manifests itself primarily through the overestimation of H. The VAR-FR approach also tends to overestimate both H and LE at the MONSOON sites owing to the underestimation of G_F at these sites.

5. Summary and Conclusions

The analysis in Section 4 demonstrates the promise, and potential limitations, of utilizing surface radiometric temperature observations (T_s) and variational data assimilation to simultaneously retrieve both surface evaporative fraction (E_F) and turbulent transfer coefficients ($(C_H)_N$ or e^R). The

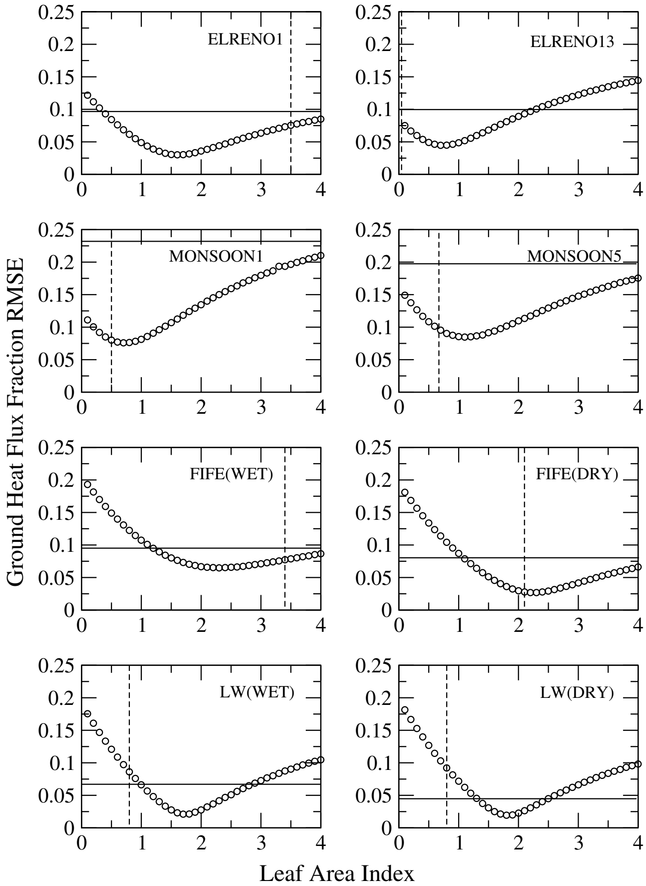

Figure 12. Comparisons between the accuracy of VAR-FR G_F prepdictions (solid horizontal lines) and TSM predictions (open circles) made using a range of L_{AI} values. Dashed vertical lines represent estimates of L_{AI} derived from NDVI values listed in Table 1 and Equation (13).

key limitation of the VAR-FR approach presented by Caparrini et al. (2003, 2004) is its tendency to be ill-posed for certain land cover types. At these sites, a continuum of R and E_F possibilities exists that produces essentially identical T_s RMSE fitness in model predictions (Figures 1–3). Minima in T_s RMSE can be sufficiently shallow such that large changes in R (and E_F) induce only negligible variations in T_s RMSE (Figures 3b and c). Retrievability problems are the most pronounced for sites exhibiting small and non-variable $T_s - T_a$ differences (Figure 5), a tendency typically associated with densely vegetated and wet surfaces. Unless addressed, retrievability problems for these surfaces will make VAR-FR predictions sensitive to even small random perturbations in T_s measurements and prevent the robust retrieval of surface energy fluxes.

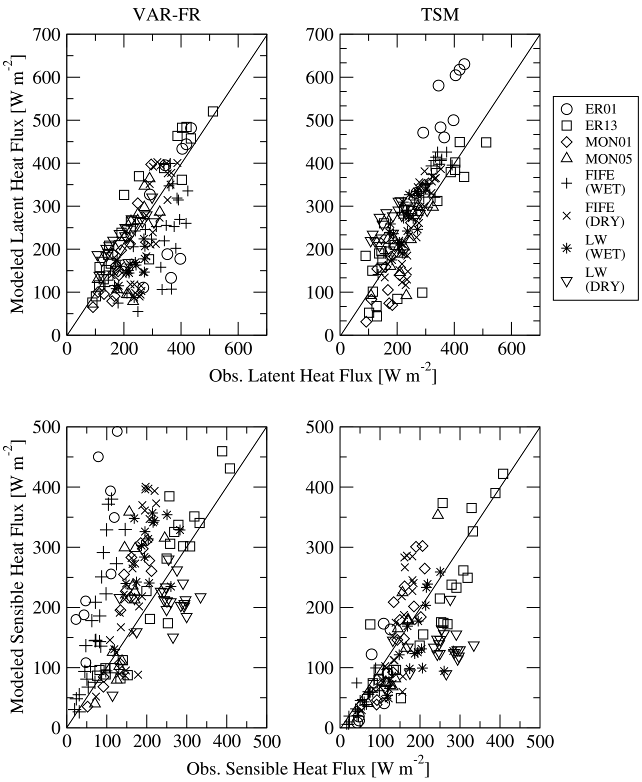

Figure 13. Scatterplot of TSM and VAR-FR H and LE predictions versus flux tower observations from all study sites. Plotted points are average flux values between 1000 and 1600 local time.

The VAR-FR approach also suffers from generic limitations impacting all single-source energy balance approaches over partially vegetated canopies. Results in Figure 7 demonstrate the sensitivity of VAR-FR R retrievals to variations in fractional vegetation coverage – due ostensibly to look angle changes – at the sparsely vegetated MONSOON1 site. The dependence of R on vegetation coverage fraction is not reflected in its physical definition and will complicate efforts to physically interpret results and/or constrain parameters within physically realistic ranges. Despite ambiguities in the physical definition of R, values retrieved by minimizing T_s RMSE predict R values that minimize the E_F error (Figure 8) reasonably well. That is, there is a tendency for T_s RMSE minima in Figure 3b to correspond to E_F RMSE minima in Figure 3c. In addition, VAR-FR E_F predictions, at least at the MONSOON1 site, are surprisingly robust to variations in vegetation coverage fraction. The impact of look angle variations is generally confined to altering R retrievals (Figure 7).

Results in Figures 11 and 12 provide a sense as to how accurately L_{AI} values must be estimated in order for the more physically complex TSM to outperform the more parsimonious VAR-FR approach. For E_F, using estimated L_{AI} values estimated from remote NDVI observations, the TSM significantly outperforms the VAR-FR approach over wet and heavily vegetated sites (e.g. ELRENO1 and FIFE(wet)), and does slightly better for partially vegetated conditions at the MONSOON5 site and LW(WET) case. In contrast, VAR-FR E_F predictions appear more accurate for the bare soil site (ELRENO13) and dry conditions at the LW site. However, the residual uncertainty concerning the true location of T_s RMSE minima in Figure 4, and therefore VAR-FR E_F predictions, complicates efforts to unambiguously rank the approaches. Relative to VAR-GR E_F predictions, uncertainty surrounding true T_s minima imparts much less uncertainty on VAR-FR G_F predictions (Figure 10). Nonetheless, results in Figure 12 provide no evidence that the more physically based G_F calculations made by the VAR-FR approach are superior to the empirical formulation used by the TSM.

Taken as a whole, VAR-FR results point towards the need for ancillary land cover information to guarantee a well-posed inversion problem and the robust prediction of surface energy fluxes results by the VAR-FR approach. Surface temperature observations alone are not sufficient to unambiguously constrain both E_F and R over partial and heavily vegetated surfaces. However, it is possible that simple and relatively robust *ad hoc* rules concerning 'reasonable' E_F and R conditions for various land surfaces may offer substantial improvement. One possibility is tighter constraints on the range of E_F values deemed physically realistic at a given site. Figure 4 demonstrates the benefits for R retrievability of constraining E_F predictions within smaller ranges. Another possibility is the specification of physically realistic ranges for R, and thus surface roughness, for various land cover types (Section 4.1). Future research should be orientated towards addressing this need.

Acknowledgements

The authors would like to thank Dara Entekhabi (MIT) for making the MATLAB code for the VAR-FR model available and Tilden Meyers of NOAA/ATDD for flux tower data at the Little Washita site.

References

Anderson, M. C., Norman, J. M., Diak, G. R., Kustas, W. P., and Mecikalski, J.R.: 1997, 'A Two-Source Time-Integrated Model for Estimating Surface Fluxes from Thermal Infrared Satellite Observations', *Remote Sens. Environ.* **60**, 195–216.

Bastiaansen, W., Menenti, M., Feddes, R., and Holtslag, A.: 1998, 'A Remote Sensing Surface Energy Balance Algorithm for Land (SEBAL) 1. Formulation', *J. Hydrol.* **212–213**, 198–212.

Betts, A. K. and Ball, J. H.: 1998, 'FIFE Surface Climate and Site-Averaged Dataset 1987–1989', *J. Atmos. Sci.* **55**, 1091–1108.

Boni, G. D., Castelli, F., and Entekhabi, D.: 2001, 'Sampling Strategies and Assimilation of Ground Temperature for the Estimation of Surface Energy Fluxes', *IEEE Trans. Geosci. Rem. Sens.* **39**, 165–172.

Boni, G. D., Entekhabi, D., and Castelli, F.: 2000, 'Land Data Assimilation with Satellite Measurements for the Estimation of Surface Energy Balance Components and Surface Control of Evaporation', *Water Resour. Res.* **37**, 1713–1722.

Caparrini, F., Castelli, F., and Entekhabi, D.: 2003, 'Mapping of Land-Atmosphere Heat Fluxes and Surface Parameters with Remote Sensing Data', *Boundary-Layer Meteorol.* **107**, 605–633.

Caparrini, F., Castelli, F., and Entekhabi, D.: 2004, 'Estimation of Surface Turbulent Fluxes through Assimilation of Radiometric Surface Temperature Sequences', *J. Hydrometeorol.* **5**, 145–159.

Castelli, F., Entekhabi, D., and Caporali, E.: 1999, 'Estimation of Surface Heat Flux and an Index of Soil Moisture Using Adjoint-State Surface Energy Balance', *Water Resour. Res.* **35**, 3115–3125.

Choudhury, B. J.: 1987, 'Relationships between Vegetation Indices, Radiation Absorption, and Net Photosynthesis Evaluated by a Sensitivity Analysis', *Remote Sens. Environ.* **22**, 209–233.

Choudhury, B. J., Ahmed, N. U., Idso, S. B., Reginato, R. J., and Daughtry, C.: 1994, 'Relations between Evaporation Coefficients and Vegetation Indices Studied by Model Simulation', *Remote Sens. Environ.* **50**, 1–17.

Crago, R. D. and Brutsaert, W.: 1996, 'Daytime Evaporation and Self-Preservation of the Evaporative Fraction and the Bowen Ratio', *J. Hydrol.* **180**, 173–194.

Diak, G. R., Mecikalski, J. R., Anderson, M. C., Norman, J. M., Kustas, W. P., Torn, R. D., and DeWolf, R.L.: 2004, 'Estimating Land Surface Energy Budgets from Space: Review and Current Efforts at the University of Wisconsin-Madison and USDA-ARS', *Bull. Amer. Meteorol. Soc.* **85**, 65–78.

French, A. N., Schmugge, T. J., Kustas, W. P., Brubaker, K. L., and Prueger, J.: 2003, 'Surface Energy Fluxes over El Reno, Oklahoma Using High-Resolution Remotely Sensed Data', *Water Resour. Res.* **39**, doi:10.1029/2002WR001734.

Garratt, J. R. and Hicks, B. B.: 1973, 'Momentum, Heat, and Water Vapour Transfer to and from Natural and Artificial Surfaces', *Quart. J. Roy. Meteorol. Soc.* **99**, 25435–25446.

Hollinger, S. E. and Daughtry, C. S. T.: 1999, *Southern Great Plains 1997 Hydrological Experiment: Vegetation Sampling and Data Documentation,* Technical Report to the United States Department of Agricultural on Contract AG-58-1270-7-043.

Jiang, L. and Islam, S.: 2001, 'Estimation of Surface Evaporation Map over Southern Great Plains Using Remote Sensing Data', *Water Resour. Res.* **37**, 329–340.

Kustas, W. P. and Goodrich, D. C.: 1994, 'Preface to MONSOON'90 Special Issue', *Water Resour. Res.* **30**, 1211–1225.

Kustas, W. P. and Norman, J. M.: 1999a, 'Reply to Comments about the Basic Equations of Dual-Source Vegetation-Atmosphere Transfer Models', *Agric. For. Meteorol.* **94**, 275–278.

Kustas, W. P. and Norman, J. M.: 1999b, 'Evaluation of Soil and Vegetation Heat Flux Predictions Using a Simple Two-Source Model with Radiometric Temperature for Partial Canopy Cover', *Agric. For. Meteorol.* **94**, 13–29.

Kustas, W. P. and Norman, J. M.: 2000a, 'Evaluating the Effects of Subpixel Heterogeneity on Pixel Average Fluxes', *Remote Sens. Environ.* **74**, 327–342.

Kustas, W. P. and Norman, J. M.: 2000b, 'A Two-source Energy Balance Approach Using Directional Radiometric Temperature Observations for Sparse Canopy Covered Surfaces', *Agron. J.* **92**, 847–854.

Kustas, W. P, Blanford, J. H., Stannard, D. I., Daughtry, C. S. T., Nichols, W. D., and Weltz, M. A.: 1994, 'Local Energy Flux Estimates for Unstable Conditions Using Variance Data in Semi-Arid Rangelands', *Water Resour. Res.* **30**, 1351–1361.

Kustas, W. P., Norman, J. M., Schmugge, T. J., and Anderson, M.C.: 2004, 'Mapping Surface Energy Fluxes with Radiometric Temperature', in D. Quattrochi and J. Luvall (eds.), *Thermal Remote Sensing in Land Surface Processes*, Taylor and Francis, New York, pp. 205–253.

Kustas, W. P., Zhan, X., and Schmugge, T. J.: 1998, 'Combining Optical and Microwave Remote Sensing for Mapping Energy Fluxes in a Semiarid Watershed', *Remote Sens. Environ.* **64**, 116–131.

Norman, J. M., Kustas, W. P., and Humes, K. S.: 1995, 'A Two-source Approach for Estimating Soil and Vegetation Energy Fluxes in Observations of Directional Radiometric Surface Temperature', *Agric. For. Meteorol.* **77**, 263–293.

Priestley, C. H. B. and Taylor, R. J.: 1972, 'On the Assessment of Surface Heat Flux and Evaporation Using Large-Scale Parameters', *Mon. Wea. Rev.*, **100** 81–92.

Sellers, P. J., Hall, F. G., Asrar, G., Strebel, D. E., and Murphy, R.E.: 1992, 'An Overview of the First International Satellite Land Surface Climatology Project (ISLCP) Field Experiment (FIFE)', *J. Geophys. Res.* **97**, 18345–18371.

Shuttleworth, W. J. and Gurney, R. J.: 1990, 'The Theoretical Relationship between Foliage Temperature and Canopy Resistance in Sparse Crops', *Quart. J. Roy. Meteorol. Soc.* **116**, 497–519.

Shuttleworth, W. J. and Wallace, J. S.: 1985, 'Evaporation from Sparse Crops – An Energy Combination Theory', *Quart. J. Roy. Meteorol. Soc.* **111**, 839–855.

Su, Z.: 2002, 'The Surface Energy Balance System (SEBS) for Estimation of Turbulent Heat Fluxes', *Hydrol. Earth Syst. Sci.* **6**, 85–99.

Twine, T. E., Kustas, W. P., Norman, J. M., Cook, D. R., Houser, P. R., Meyers, T. P., Prueger, J. H., Starks, P. J., and Wesley, M. L.: 2000, 'Correcting Eddy-Covariance Flux Estimates over a Grassland', *Agric. For. Meteorol.* **103**, 279–300.

Verma, S., Kim, J., and Clement, R. J.: 1992, 'Momentum, Water Vapour, and Carbon Dioxide Exchange at a Centrally Located Prairie Site during FIFE', *J. Geophys. Res.* **97**, 18629–18639.